RSC Chemical Biology

ROYAL SOCIETY OF CHEMISTRY

COMMUNICATION

View Article Online
View Journal | View Issue

Cite this: *RSC Chem. Biol.*, 2025, 6, 1270

Received 31st May 2025,
Accepted 8th July 2025

DOI: 10.1039/d5cb00141b

rsc.li/rsc-chembio

Random peptide mixtures of tryptophan and lysine suppress the aggregation of a cancer-related mutant of the Axin protein†

Tommaso Garfagnini, [a] Zvi Hayouka [b] and Assaf Friedler *[a]

Aggregation of dysfunctional proteins can lead to a variety of diseases including cancer. We have previously developed chaperone-derived peptides that inhibit aggregation of the cancer-related L106R mutant of Axin RGS. Here we show that significantly improved inhibition was achieved using random peptide mixtures (RPMs) designed to mimic the chemical characteristics of the chaperone-like peptides. 20-mer RPMs of tryptophan and lysine suppressed aggregation of Axin RGS L106R with up to 50-fold improved activity compared to parent inhibitors. Conversely, peptides derived from the lead hotspot of Axin RGS aggregation that were designed to be specific, were unable to prevent aggregation of the protein. RPMs constitute the most efficient strategy to date to magnify peptide inhibitory activity against Axin RGS L106R aggregation, as they contain multiple active species and conformations that cover a larger inhibitory space and shield multiple hotspots at once. Our results demonstrate that the chemical composition of the peptide, and not the specific sequence, is the key factor for inhibitory activity.

Introduction

Disease-related protein aggregates pose a serious threat to human health and intensive research is performed for developing inhibitors of aggregation processes.[1] Peptides are rationally designed to target aggregating proteins with high specificity.[2] However, the simultaneous involvement of multiple paths and hotspots makes it therapeutically unviable to effectively prevent aggregation by targeting one hotspot with one peptide at a time, as was shown for the aggregation of the tumour suppressor p53.[3,4] The number of approved aggregation inhibitory drugs is indeed very small.[5] Chaperones have hence been proposed as a viable alternative thanks to their multi-targeting.[6] Specific portions of chaperones like Humanin, Hsp20/27 and αA/αBcrystallin proved sufficient for inhibiting aggregation of a variety of proteins.[7–10]

The Axin protein has emerged as a potential anti-cancer drug target for an aggregation inhibition strategy.[11] Axin is the scaffold protein that regulates the canonical Wnt pathway in the cytosol by recruiting β-catenin, the protein transducer that relays Wnt signalling from the cell surface to the nucleus and promotes transcription of pro-survival genes.[12] Axin orchestrates a dynamic, multi-client complex, termed the destruction complex, with the function of depleting β-catenin and preventing cellular outgrowth.[12] Upon Axin binding, β-catenin is phosphorylated and addressed to degradation, thereby abrogating Wnt signalling and depriving the cell of an effective tumour suppressor mechanism.[13] The RGS domain of Axin modulates β-catenin binding and determines the on/off state of Wnt signalling, directly impacting carcinogenesis.[13] The cancer-related L106R mutant of the RGS domain in Axin impairs the Wnt suppressing function of Axin and dysregulates cell fate.[11] Destabilised L106R Axin accumulates *in vivo* as soluble nanoaggregates of no more functional protein that is unable to orchestrate β-catenin degradation, resulting in hepatocellular cancer.[11,14] We have previously shown that the αBcrystallin-derived peptides ^{8}PWIRRPFFPFHSPSR^{22} and ^{45}SPFYLRPPSFLRAPSWF^{61} suppress the aggregation of Axin RGS L106R *in vitro*. Moreover, and similarly to the way full-length chaperones act, we found that inhibition is encoded not in the sequence but rather in the molecular determinants of composition (20–30% flexible, 30–40% aliphatic, 20–30% aromatic residues), hydrophobicity (equal to hydrophilicity), and distribution (non-clustered).[15]

Random peptide mixtures (RPMs) are ensembles of peptides comprising all combinations of one hydrophobic and one cationic amino acid randomly distributed.[16] RPMs selectively lyse bacterial cell membranes.[17] Being non-toxic to eukaryotic cells, RPMs proved viable antimicrobials in food and pharmaceutical industry.[18–21] The presence of many sequences

[a] *Institute of Chemistry, The Hebrew University of Jerusalem, Edmond J. Safra Campus at Givat Ram, Jerusalem 9190401, Israel. E-mail: assaf.friedler@mail.huji.ac.il*
[b] *Institute of Biochemistry, Food Science and Nutrition, The Hebrew University of Jerusalem, The Robert H. Smith Faculty of Agriculture, Food and Environment, Rehovot 76100, Israel. E-mail: zvi.hayouka@mail.huji.ac.il*

† Electronic supplementary information (ESI) available. See DOI: https://doi.org/10.1039/d5cb00141b

associated with antimicrobial properties hinders the development of resistance, and allows for broad recognition and activity against multiple bacterial strains.[22–25]

Here, to develop improved inhibitors of Axin L106R aggregation, we first designed a family of peptides based on the sequence of the main aggregation hotspot of Axin RGS L106R. Then, to develop better, multi-targeting protein aggregation inhibitors, we applied the RPMs approach to evolve the αBcrystallin-derived peptides into the next generation of Axin RGS L106R aggregation inhibitors. We generated RPMs composed of two residues that recapitulated the flexibility and π-stacking capability of the alphaBcrystallin-derived inhibitors and comprised all potential distributions with inhibitory activity. Our results show that none of the hotspot-derived peptides suppressed the early soluble aggregates that correlate with carcinogenesis. Conversely, the RPM of tryptophan and lysine (WK) suppressed Axin RGS L106R aggregation in a molar ratio of 1 : 1 protein : peptide, outperforming the hotspot-derived peptides and substantially improving the activity of all αBcrystallin-derived peptides.

Results

Design of hotspot-derived peptides

Previous work to determine the molecular mechanism of Axin RGS L106R aggregation and its causative link with related carcinogenesis identified the stretch ^{116}DFWFACTGF^{124} as the leading hotspot that is responsible for aggregation both *in vitro* and *in vivo*, and for the onset of the cancer phenotype.[11] We then set out to design peptides that target specifically the ^{116}DFWFACTGF^{124} hotspot and test whether that is a viable strategy to obtain comprehensive inhibition of Axin RGS L106R aggregation. Recently, the sequence ^{113}DLLDFWFACTGFRKL^{127} (Axin 113–127), which contains this hotspot, was found capable of Axin RGS L106R binding on a peptide array.[15] Axin 113–127 was hence our starting point to develop Axin RGS-specific peptides that inhibit aggregation by associating with the hotspot and blocking its interactions. However, the wild type sequence of the Axin 113–127 peptide proved insoluble. The presence of one cysteine residue increases the risk of oxidation and oligomerisation, while electrostatic neutrality due to the presence of two negatively charged and two positively charged residues allows for the self-association of the hydrophobic core of the peptide. Thus we designed variants to increase the solubility with minimal changes in the natural sequence to preserve and improve its binding and activity (Table 1). SP-Axin 113–127 was designed to have cysteine substituted to serine to prevent disulfide bonding, and glycine substituted to proline to disfavour hydrophobic collapse thanks to the properties of proline as an aggregation-breaker.[26,27] In RS-Axin 113–127 all negatively charged residues were substituted to arginine, while DS-Axin 113–127 had all positively charged residues substituted to aspartic acid. Arginine was the cationic residue of choice because it is strongly enriched over lysine in peptide inhibitors of Axin RGS L106R aggregation.[15] Conversely, aspartic acid was chosen for its higher solubility compared to glutamic acid. Finally, we sought to identify minimal inhibitors of Axin RGS L106R aggregation that spanned the hydrophobic core of the hotspot only. Truncated versions were hence produced: S-Axin 115–121, with a cysteine mutated to serine, and RS-Axin 115–121, that incorporated also a charge switch with an aspartic acid substituted to arginine (Table 1).

Table 1 Peptides based on the RGS aggregation hotspot[a]

Peptide	Sequence
Axin 113–127	DLLDFWFACTGFRKL-NH_2
SP-Axin 113–127	DLLDFWFASTPFRKL-NH_2
RS-Axin 113–127	RLLRFWFASTGFRKL-NH_2
DS-Axin 113–127	DLLDFWFASTGFDDL-NH_2
S-Axin 115–121	LDFWFAS-NH_2
RS-Axin 115–121	LRFWFAS-NH_2

[a] The positive (blue), negative (red), and aromatic (yellow) residues are highlighted.

In vitro characterisation of peptide inhibition of Axin RGS L106R aggregation

We first tested the effect of the peptides on Axin RGS L106R aggregation using 1-anilinonaphthalene-8-sulfonic acid (ANS) fluorescence. This assay was selected as the first screening assay because it provides specific information on the soluble aggregates formed early in the aggregation process. These are the aggregated species that are responsible for the molecular aetiology of carcinogenesis following L106R aggregation: the cancer phenotype *in vivo* is caused by soluble nano-bundles of aggregated protein that prevent the formation of a functional destruction complex, far before the appearance of the mature, extended aggregates observed *in vitro*.[11] ANS is sensitive to hydrophobic environments and it undergoes an increase in the emission at 470 nm upon binding to the hydrophobic patches exposed on protein surface.[28] As such, ANS detects monomeric partially unfolded proteins, soluble misfolded oligomers and early aggregates, proving suitable for tracking the emergence of the whole spectrum of intermediate states of protein aggregation before mature aggregates are formed.[29–32] It can thus selectively monitor the early phase of protein aggregation in the case of Axin RGS L106R.

Axin RGS L106R aggregation in the absence and in the presence of peptides was followed by time course kinetics of ANS emission at 470 nm. The kinetics traces were fit to a single exponential equation and the rate constant (k_{ANS}) was determined to characterise the early aggregation process (eqn (1), Materials and methods). The kinetic constants k_{ANS} were used as a semi-quantitative screening to identify the peptides that exerted an inhibitory activity on the early phase of aggregation. The increase in k_{ANS} reflected the stabilization and rapid accumulation of hydrophobic intermediates of Axin RGS L106R aggregation, as the peptides prevented further aggregation and subsequent burial of the ANS-binding sites within larger aggregates.[15] However, ANS is not specific for any particular species on the aggregation path, and k_{ANS} cannot identify

which aggregation intermediate the peptides target or the eventual outcome of their inhibition. Therefore, it does not provide fully quantitative information about the aggregation process. In the next step, TEM was systematically employed as a quantitative method to validate inhibition and provide structural details on Axin RGS L106R aggregation and its inhibition.

Axin RGS L106R aggregation induced a marked increase in ANS emission at 470 nm over time, with a k_{ANS} of 0.58 ± 0.09 μM^{-1} h^{-1} that was compatible with previous reports.[15,33] The absence of a lag phase is consistent with the probe detecting not just the aggregates but all intermediate states from the very start of the aggregation process. TEM imaging confirmed the formation of extended aggregates of Axin RGS L106R in the absence of peptides, capturing in detail their worm-like, unbranched morphology recently characterised.[15,33] RS-Axin 113–127 substantially enhanced k_{ANS} of Axin RGS L106R aggregation to 3.12 ± 0.34 μM^{-1} h^{-1}, 5.4-fold higher than in the absence of peptide, at 8 μM and 1 : 1 protein : peptide molar ratio. In connection with the observed increase in k_{ANS}, TEM imaging revealed that aggregation was only partially inhibited by RS-Axin 113–127 (Fig. 1C and Fig. S2A, ESI†). A high number of small oligomers in the size of 5–10 nm were observed, together with a few large, thick aggregates possibly resulting from the association of the oligomers (Fig. 1C). This is compared to 50–150 nm high aggregates formed by Axin RGS L106R in the absence of peptides. TEM imaging hence validated that the increase in k_{ANS} significantly correlates with a stabilization of oligmeric intermediate states of Axin RGS L106R and an overall inhibitory effect on aggregation (Fig. 1A, C and Table 2). In particular, based on the oligomeric assemblies observed by TEM, the combination of high values of k_{ANS} and ANS emission at the plateau suggested that RS-Axin 113–127 stabilised late hydrophobic intermediates. Indeed, on one hand the hotspot-derived peptide was unable to completely inhibit aggregation because it did not target and shield all secondary hotspots with different amino acid sequence (Fig. 1A). On the other hand, sealing the main aggregation hotspot prevented the formation of mature aggregates, as the hydrophobic patches remained exposed to the solvent and available for ANS binding, without being buried in a growing aggregate.

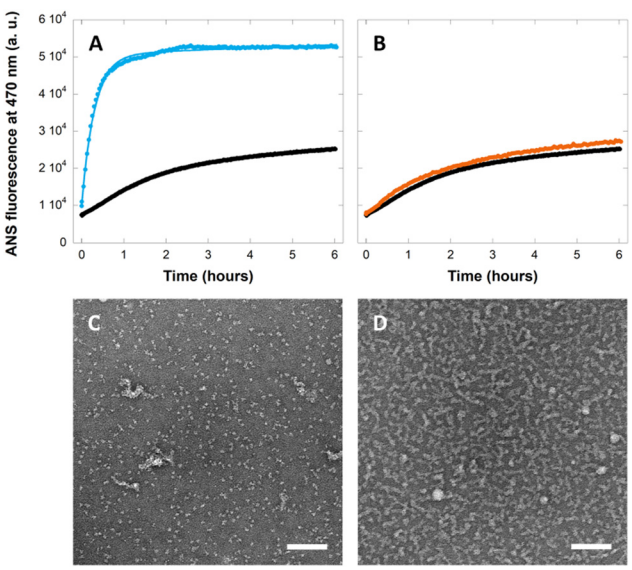

Fig. 1 Effect of hotspot-derived peptides on Axin RGS L106R aggregation. ANS aggregation kinetics of 8 μM Axin RGS L106R in the absence (black) or in the presence of (A) 8 μM RS-Axin 113–127 (light blue) and (B) 80 μM DS-Axin 113–127 (orange). The traces were acquired in triplicates. TEM imaging of RGS L106R aggregates incubated for 12 hours at 25 °C with 8 μM (C) RS-Axin 113–127 or (D) DS-Axin 113–127. The scale bar equals 100 nm.

Table 2 Effect of the peptides on Axin RGS L106R aggregation

Peptide	k_{ANS} (μM^{-1} h^{-1})	TEM observation
No peptide	0.58 ± 0.09	50–150 nm high aggregates
RS-RGS 113–127	3.12 ± 0.34	Inhibition
DS-RGS 113–127	0.65 ± 0.12	No effect or mild effect
WK	2.0 ± 0.32	Suppression
YK	1.48 ± 0.13	Size/shape-control

DS-Axin 113–127 poorly affected the ANS kinetics of Axin RGS L106R aggregation (Fig. 1B and Table 2). This was supported by TEM imaging, that revealed the formation of a larger number of aggregates with a branched morphology (Fig. 1D). SP-Axin 113–127, S-Axin 115–121 and RS-Axin 115–121 had no effect on Axin RGS L106R aggregation (Fig. S1, ESI†). The peptides alone did not form aggregates (Fig. S2D–F, ESI†). The hotspot-derived peptides hence failed to achieve complete suppression of Axin RGS L106R aggregation.

Design of RPMs that mimic the molecular determinants of chaperone-derived peptides

Although partial inhibition was achieved with RS-Axin 113–127, the hotspot-derived peptide failed at preventing the formation of the early oligomeric aggregates that are responsible for the cancer phenotype. We then pursued an alternative approach, and designed inhibitors that act irrespective of the sequence of the Axin hotspot and have the potential of shielding multiple hotspots. We based on our previous study, showing that the αBcrystallin_8-22 peptide inhibits the aggregation of Axin RGS L106R by exerting a chaperone-like activity, without being specific for the ^{116}DFWFACTGF^{124} hotspot.[15] We used this peptide as a starting point for developing binary random peptide mixtures (RPMs) that mimicked the molecular determinants of chaperone-like inhibitory activity.[15] The RPMs were set to have the same π–stacking capacity and flexibility as αBcrystallin_8–22. Arginine, histidine, tryptophan and phenylalanine are collectively responsible for π-stacking interactions and account for 53.3% of αBcrystallin_8–22 sequence. Arginine and proline confer flexibility *via* electrostatic repulsion and torsion angle, comprehensively accounting for 46.7% of the sequence. Previous screenings also revealed that maximising the number of residues with both π-stacking and H-bonding capacity increased the inhibitory activity of αBcrystallin_8–22.[15] We thus designed RPMs containing one aromatic and one charged residue to mimic such molecular properties. The π-stacking/H-bonding capacity was recapitulated with tryptophan

or tyrosine, and the flexibility with the oppositely charged residues lysine or glutamic acid. Lysine was the positively charged residue of choice because of the higher tendency of arginine to participate in π–cation interactions with aromatic residues, and particularly tryptophan, which can establish intramolecular interactions that hinder the potency of the RPMs as aggregation inhibitors.[34] In addition, polyarginine peptides self-associate *via* ion salt bridges, meaning that arginine-rich stretches display attractive interactions that may impair protein targeting, while lysine exclusively generates repulsive interactions.[35] Binary peptides of an aromatic residue and arginine indeed are known to self-assemble into ordered aggregates and insoluble fibers.[36] To best mimic the chaperone-derived peptides αBcrystallin_8–22 (15 aa), αBcrystallin_45–61 (17 aa), Clusterin_200–221 and Clusterin_216–237 (22 aa), we set 20, the closest average even number of residues, as the RPMs length.[15] So, we generated four 20-mer binary RPMs: tryptophan/lysine (WK), tyrosine/lysine (YK), tryptophan/glutamic acid (WE), and tyrosine/glutamic acid (YE).

As previously described, each binary RPM constituted an ensemble of peptides sequences comprising all possible combinations of the two residues of choice (see Materials and methods).[16,17] Given the probabilistic nature of randomised peptide coupling, the majority of the peptides within the RPM contained 50% of one residue and 50% of the other, without a fixed distribution. Compared to the progenitor αBcrystallin_8–22 inhibitor, the advantage of RPMs was to generate the widest variety of hydrophobic, aromatic and charge patterns associated with inhibitory activity within a single sample, achieved by shuffling two residues throughout the sequence. Although not all peptides in the RPM are active, the sequence pool likely included peptides with diverse distributions capable of targeting multiple hotspots with varying composition.

Complete suppression of Axin RGS L106R aggregation by WK

Two RPMs, WK and YK, induced a steep acceleration of the ANS kinetics of Axin RGS L106R aggregation at 8 μM and 1 : 1 protein : peptide molar ratio. In the presence of WK the k_{ANS} increased to 2.0 ± 0.32 μM^{-1} h^{-1}, which corresponded approximately to a 3.5-fold higher value than the absence of RPM (Fig. 2A, B and Table 2). Such a k_{ANS} increase, together with the low ANS emission at 12 hours of aggregation kinetics, suggested the stabilisation of an early precursor of the aggregation process. The addition of YK resulted in a k_{ANS} of 1.48 ± 0.13 μM^{-1} h^{-1}, that constituted a 2.6-fold increase in the rate of the accumulation of hydrophobic intermediates (Fig. 2A, B and Table 2). The lower k_{ANS} value of YK compared to WK was indicative of YK being unable to fully prevent aggregation and exerting its stabilisation action at a later stage, where an aggregate is formed. Consistently with the observed values of k_{ANS}, TEM imaging revealed that WK suppressed Axin RGS L106R aggregation almost completely, with only small round assemblies indistinguishable from a grid loaded with Axin RGS WT[33] (Fig. 2C). YK stabilised oligomeric species and exerted a tight size and shape control over such Axin RGS L106R early aggregates, preventing their further assembly into mature aggregates. Indeed, YK determined the formation of compact, spherical assemblies with a height between 10 and 20 nm, as opposed to the 50–150 nm high worm-like aggregates formed without peptides (Fig. 2D and Fig. S2A, ESI†).

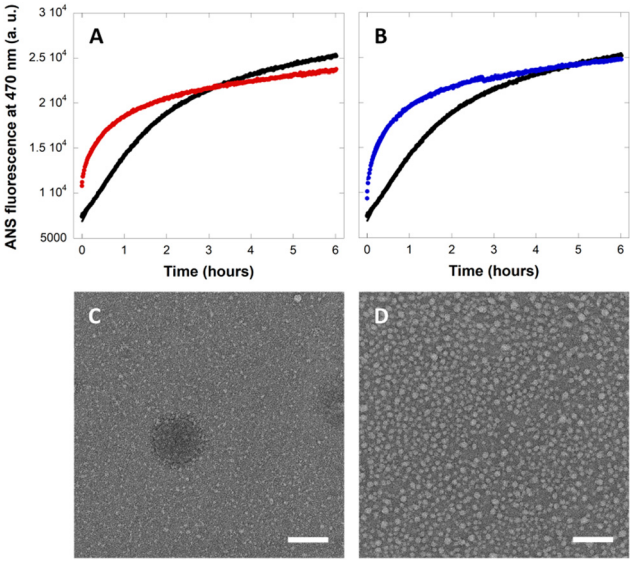

Fig. 2 Effect of WK and YK on Axin RGS L106R aggregation. ANS aggregation kinetics of 8 μM Axin RGS L106R in the absence (black) or presence of 8 μM (A) WK (red) and (B) YK (blue). The traces were acquired in triplicates. TEM imaging of Axin RGS L106R aggregates incubated for 12 hours at 25 °C with 8 μM (C) WK or (D) YK. The scale bar equals 100 nm.

Conversely, WE and YE enhanced the aggregation of Axin RGS L106R in terms of both number and size of the aggregates. In addition, the aggregates displayed substantial morphological differences compared to those formed in the absence of peptides. WE induced the formation of a larger number of thin Axin RGS L106R aggregates between 30 and 50 nm high that retained the worm-like, unbranched morphology (Fig. 3A and Fig. S2A, ESI†). The co-incubation with YE yielded thick worm-like aggregates 100 nm or more high, that were also branched, as well as spheroidal oligomers about 5–10 nm high (Fig. 3B and Fig. S2A, ESI†). WE and YE RPMs alone did not aggregate (Fig. S2B and C, ESI†).

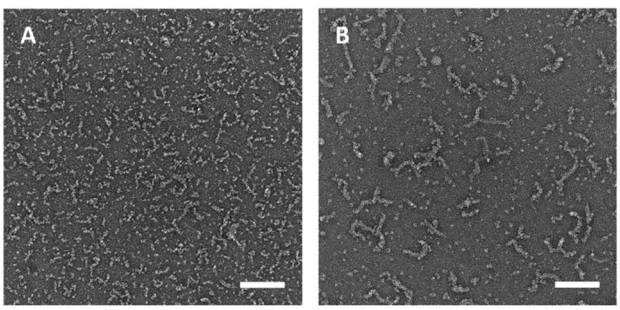

Fig. 3 Effect of WE and YE on Axin RGS L106R aggregation. TEM imaging of Axin RGS L106R aggregates incubated for 12 hours at 25 °C with 8 μM (A) WE or (B) YE. The scale bar equals 100 nm.

Discussion

Our results show that WK effectively inhibited Axin RGS L106R aggregation at 8 μM and 1 : 1 protein : peptide molar ratio. This is a significantly improved activity compared to the chaperone-derived peptides αBcrystallin_8–22, which is progenitor of the designed RPMs, and αBcrystallin_45–61. Complete suppression of aggregation was observed only at 400 μM αBcrystallin_8–22 (1 : 50 molar ratio), and 120 μM αBcrystallin_45–61 (1 : 15 molar ratio).[15] WK also outperformed the optimised, tryptophan-enriched W/T-αBcrystallin_8–22 peptide that suppressed aggregation at 32 μM (1 : 4 molar ratio).[15] In addition, WK exhibits an average hydrophobicity/hydrophilicity ratio (ψ) of 0.8, calculated using the Roseman hydrophobicity scale.[37] This value aligns closely with the molecular determinant known to confer anti-aggregation activity in chaperone-derived inhibitors.[15] In contrast, with ψ = 0.5, YK exhibits intermediate suppression activity by modulating aggregation and redirecting it into size-controlled spherical assemblies. The complete suppression by WK can then be attributed to its alignment with the rational design criteria, and its superior performance is likely due to its closer resemblance to the molecular determinants that guided the design strategy.

Since chaperone-derived peptides were the starting point for developing the RPMs, we expect WK to behave similarly to the parent αB-crystallin chaperone with its clients in the living cell: engaging in broad yet selective interactions.[15] Like αBcrystallin, WK may interact with various proteins not based on sequence specificity, but preferentially binding to misfolded or aggregation-prone species. In the case of Axin RGS variants, WK will then target the mutated protein like a chaperone, selectively interacting with exposed aggregation hotspots while interacting only weakly, if at all, with the folded wild-type. This chaperone inspired strategy for RPM design hence reduces the likelihood of interference with normal cellular function.

The fact that WK suppresses Axin RGS L106R aggregation is also efficiently supported by our previous finding that positively charged chaperone-derived peptides enriched in tryptophan have an enhanced inhibitory activity.[15] WK hence likely maximised the inherent multi-targeting inhibition exerted by such peptides. A possible reason for the augmented inhibitory potency could be that, diversely from the chaperone-derived peptides, WK is constituted by a multiplicity of amino acid sequences and distributions, all of which potentially endowed with inhibitory activity. The RPM hence generates a wide range of inhibitors that can display affinity for different hotspots with different composition or molecular properties. As a result, WK may target multiple hotspots at once and quench their aggregative potential collectively by using different sequences of the mixture (Fig. 4).

WK was also a better inhibitor than peptides specifically designed to mimic and target the ^{116}DFWFACTGF^{124} aggregation hotspot of Axin RGS L106R. Indeed, RS-Axin 113–127 at 8 μM (1 : 1 molar ratio) was only able to decrease the size of the aggregates, without fully suppressing aggregation. This reinforces the idea that targeting multiple hotspots at once is the most likely mechanism of action for the RPMs, and a more effective strategy to obtain inhibition than targeting aggregation *via* a single hotspot. By encompassing a pool of sequences with different conformations and degrees of affinities, an RPM inhibitor can dynamically seal a wider variety of hotspots and result in a comprehensive protection against aggregation (Fig. 4). Conversely, YK did not suppress aggregation, probably due to the lower hydrophobicity of tyrosine. YK shape/size control over Axin RGS L106R aggregates is reminiscent of the effect of sucrose and may depend on the high density of hydroxyl groups.[33] WK hence constitutes a promising alternative to designed peptides inhibitors of Axin RGS L106R aggregation. These findings further support the notion that the amino acid composition of an aggregation inhibitor is more important than its sequence for activity.

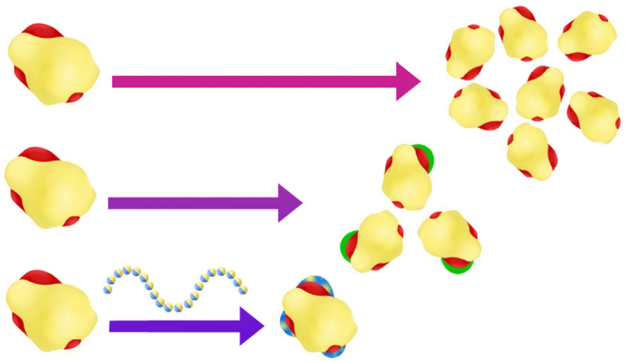

Fig. 4 Mechanism of peptide inhibition of Axin RGS L106R aggregation. In the absence of peptides, Axin RGS L106R forms native-like aggregates led by multiple hotspots (red patches). The hotspot-derived peptide RS-Axin 113–127 (green capping) targets the parent ^{116}DFWFACTGF^{124} hotspot and shields it, but it is unable to stop aggregation from secondary hotspots, so it stabilizes smaller aggregates bound together by weaker interactions. WK (blue-yellow cappings, diversely shaded as to account for varying RPM compositions and distributions) targets all hotspots at once using different sequences of the mixtures, hence obtaining full inhibition of aggregation.

Positive charges proved key for WK activity, as for other aggregation inhibitors. For example, the synthetic polycation poly-*N*-ethyl-4-vinylpyridine bromide is an effective protein aggregation inhibitor thanks to the high positive charge, aromacity, and sp^2 Nitrogen H-bonding, that make it reminiscent of WK.[38] Lysine further contributes by preventing the intermolecular interactions between misfolded or partially folded states.[39,40] These effects are consistent with the WK-mediated suppression of Axin RGS L106R aggregation *via* stabilisation of a precursor state. Negative charges, that play a major role in chaperoning by natural and synthetic polyanions, were instead heavily detrimental for the inhibitory activity of both hotspot-derived peptides and RPMs.[41,42]

Conclusions

In conclusion, converting individual sequences of peptides into RPMs proved a successful strategy to obtain powerful inhibitors of Axin RGS L106R aggregation. Being active regardless of

specific hotspots, WK may act as a lead compound to develop new inhibitors of Axin RGS related cancers and a platform for screening randomised-sequence therapies. It could also act as chaperone-like stabilisers in bioformulations or as generic probes for sensing protein aggregates.

Materials and methods

Protein expression and purification

Axin RGS L106R was expressed and purified as described.[33] Briefly, pGEX-2T vector was modified with TEV cleavage site and inserted with Axin RGS L106R gene. BL21 codon plus cells were transformed and grown in LB media at 37 °C in the presence of ampicillin and chloramphenicol until an $[OD]_{600}$ of 0.6. Expression was induced with 0.6 mM isopropyl β-D-1-thiogalactopyranoside overnight at 16 °C. The bacteria were resuspended in 50 mM Tris HCl pH 7.4, 300 mM NaCl, 5 mM β-mercaptoethanol, 10 μg mL^{-1} DNAase, 10 μg mL^{-1} lysozyme and 1 mM phenylmethanesulfonyl fluoride and lysed using a microfluidiser. Axin RGS L106R was separated at 15 000 rpm, purified with Merck GST-bind 70 541 resin, cleaved with TEV protease overnight at 4 °C, and further purified by ÄKTA-assisted size exclusion chromatography with two coupled Superdex75 and Superose12 200 mL columns. The protein was concentrated, filtered on 0.22 μm cut-off filters and stored at −80 °C.

Peptide synthesis

The hotspot-derived peptides were synthesised with a 9-fluorenylmethoxycarbonyl (Fmoc) chemistry using a Liberty Microwave Assisted Peptide Synthesizer (CEM, Matthews, NC, USA). *N*,*N*′-diisopropylcarbodimide (DIC)/oxyma coupling reagents and Rink-Amide resin with 0.546 mmol g^{-1} substitution were employed. The peptide synthesis was performed at a scale of 0.1 mmol in the presence of 0.4 mmol amino acids, 1.0 mmol oxyma and 0.8 mmol DIC, using dimethylformamide (DMF) as solvent. Fmoc deprotection was performed using a 20% (v/v) piperidine solution in DMF. The cleavage from the resin was performed in 95% (v/v) trifluoroacetic acid (TFA), 2.5% (v/v) triisopropylsilane (TIS), 2.5% (v/v) triple distilled water (TDW) under agitation for 3 hours at room temperature. After partial evaporation, the peptides were precipitated adding 4 volumes of diethylether at −20 °C. The precipitate was sedimented for 30 minutes at −20 °C, washed three times with diethylether, dried, dissolved in 1 : 2 acetonitrile (ACN) : TDW solution, flash-frozen in liquid nitrogen and lyophilized. The peptides were purified with a reverse-phase C18 preparative column on a Jasco LG2080 HPLC operating a 10-to-40% (v/v) ACN:TDW gradient at a rate of 0.5%/min. The peptides were identified by determining their exact mass using MALDI-TOF mass spectrometry (Bruker Daltonik, Germany). The peptides purity was validated by Merck Hitachi D7000 analytical HPLC equipped with a reverse-phase C8 analytical column (Fig. S3 and Table S1, ESI†).

The binary random peptide mixtures (RPMs) were synthesized as described.[16,17] Briefly, equimolar solutions of tyrosine and lysine, tyrosine and glutamic acid, tryptophan and lysine or tryptophan and glutamic acid were prepared for coupling. Fmoc chemistry and same activants conditions were employed as for the hotspot-derived peptides. At each synthesis cycle, the two amino acids of the solution had the same probability to undergo coupling. As a consequence of a randomised coupling, the final product was a mixture of peptides comprising all possible combinations of sequences of the two amino acids of choice. The cleavage was performed as described for the hotspot-derived peptides. The RPMs were used after lyophilisation. RPMs concentration was determined using an averaged molecular weight calculated for a peptide sequence constituted by 50% of each constituent amino acid (Fig. S4 and Table S2, ESI†).

UV spectroscopy

Protein and ANS quantification was performed by UV spectroscopy using a Shimadzu UV-1650PC and a quartz cuvette of 0.1 cm path length. Axin RGS L106R extinction coefficient at 280 nm (ε_{280}) was 0.936 M^{-1} cm^{-1}, as computed by ExPASy ProtParam. ANS extinction coefficient at 360 nm (ε_{360}) was 5700 M^{-1} cm^{-1}, as previously reported.[43]

ANS fluorescence

ANS kinetics were acquired using a BioTek Synergy H1 Hybrid Reader (Thermo Scientific) plate reader and 96 wells half-area plates (Costar 3696). Excitation wavelength was 380 nm and the emission was recorded at 470 nm. 75 μL of aggregating solution containing 32 μM ANS in the absence or in the presence of peptides at different concentrations were incubated at 25 °C. 25 μL of 32 μM Axin RGS L106R solution kept on ice were added to the wells pipetting 3 times to homogenise, to final conditions 8 μM Axin RGS L106R, 24 μM ANS, 50 mM Tris HCl pH 7.4, 150 mM NaCl, 5 mM β-mercaptoethanol. All kinetics were performed at 25 °C.

Data analysis

ANS kinetics throughout 12 hours of incubation in the absence or in the presence of peptides were fit with an exponential plus line equation:

$$y = m_0 + m_1 \cdot t + m_2 \cdot \exp(-k_{ANS} \cdot t) \quad (1)$$

where m_0 is the ANS emission at 12 hours; m_1 is the slope of the linear term correcting for the absence of a plateau at long times; m_2 is the difference between ANS emission at the end and at the beginning of the kinetics; k_{ANS} is the rate constant of the exponential growth phase and t is time.

Transmission electron microscopy

8 μM Axin RGS L106R were incubated in the absence or in the presence of 8 μM peptides for 12 hours, at 25 °C. Alternatively, 8 μM peptides were incubated in the absence of protein in the

same conditions. The aggregation reaction solution was diluted 10x and 3 to 5 μL were applied to a glow discharged TEM grid (carbon supported film on 300 mesh Cu grids, Ted Pella, Ltd.). After 30 s the excess liquid was blotted, the grids stained with 2% uranyl acetate for 30–60 s, blotted and allowed to dry in air. The samples were examined using FEI Tecnai 12 G2 TWIN TEM operated at 120 kV. The images were recorded by a 4 K × 4 K FEI Eagle CCD camera. In all solutions the buffer was 50 mM Tris HCl pH 7.4, 150 mM NaCl, 5 mM β-mercaptoethanol.

Conflicts of interest

The authors declare no conflicts of interest.

Data availability

The data supporting this article have been included as part of the ESI.†

Acknowledgements

The research was supported by the Innovative Training Network 608180 ''WntsApp'' by the Marie-Curie Actions of the 7th Framework program of the EU. AF thanks the support of the Minerva Center for Bio-Hybrid complex systems and the Saerree K and Louis P Fiedler Chair in Chemistry. We thank Yeal Levi-Kalisman and the Harvey M Krueger Family Center for Nanoscience and Nanotechnology for TEM imaging.

Notes and references

1 C. M. Dobson, T. P. J. Knowles and M. Vendruscolo, *Cold Spring Harb. Perspect. Biol.*, 2020, **12**, a033878.
2 V. Armiento, A. Spanopoulou and A. Kapurniotu, *Angew. Chem., Int. Ed.*, 2020, **59**, 3372–3384.
3 G. Wang and A. R. Fersht, *Proc. Natl. Acad. Sci. U. S. A.*, 2015, **112**, 2443–2448.
4 G. Z. Wang and A. R. Fersht, *Proc. Natl. Acad. Sci. U. S. A.*, 2017, **114**, E2634–E2643.
5 M. Perni and B. Mannini, *Biomolecules*, 2024, **14**, 1324.
6 M. E. Jackrel and J. Shorter, *Front. Neurosci.*, 2017, **11**, 99.
7 A. K. Okada, K. Teranishi, F. Lobo, J. M. Isas, J. Xiao, K. Yen, P. Cohen and R. Langen, *Sci. Rep.*, 2017, **7**, 7802.
8 R. B. Nahomi, M. A. DiMauro, B. Wang and R. H. Nagaraj, *Biochem. J.*, 2015, **465**, 115–125.
9 N. Tanaka, R. Tanaka, M. Tokuhara, S. Kunugi, Y. F. Lee and D. Hamada, *Biochemistry*, 2008, **47**, 2961–2967.
10 J. Bhattacharyya, E. G. P. Udupa, J. Wang and K. K. Sharma, *Biochemistry*, 2006, **45**, 3069–3076.
11 Z. Anvarian, H. Nojima, E. C. Van Kappel, T. Madl, M. Spit, M. Viertler, I. Jordens, T. Y. Low, R. C. Van Scherpenzeel, I. Kuper, K. Richter, A. J. R. Heck, R. Boelens, J. P. Vincent, S. G. D. Rüdiger and M. M. Maurice, *Nat. Struct. Mol. Biol.*, 2016, **23**, 324–332.
12 M. M. Maurice and S. Angers, *Nat. Rev. Mol. Cell Biol.*, 2025, **26**, 371–388.
13 J. M. Bugter, N. Fenderico and M. M. Maurice, *Nat. Rev. Cancer*, 2021, **21**, 5–21.
14 K. Taniguchi, L. R. Roberts, I. N. Aderca, X. Dong, C. Qian, L. M. Murphy, D. M. Nagorney, L. J. Burgart, P. C. Roche, D. I. Smith, J. A. Ross and W. Liu, *Oncogene*, 2002, **21**, 4863–4871.
15 T. Garfagnini, L. Ferrari, M. B. Koopman, F. A. Dekker, S. Halters, E. Van Kappel, G. Mayer, S. Bressler, M. M. Maurice, S. G. D. Rüdiger and A. Friedler, *Chem. – Eur. J.*, 2024, **30**, e202400080.
16 Z. Hayouka, S. Chakraborty, R. Liu, M. D. Boersma, B. Weisblum and S. H. Gellman, *J. Am. Chem. Soc.*, 2013, **135**, 11748–11751.
17 Z. Hayouka, A. Bella, T. Stern, S. Ray, H. Jiang, C. R. M. Grovenor and M. G. Ryadnov, *Angew. Chem., Int. Ed.*, 2017, **56**, 8099–8103.
18 Z. Amso and Z. Hayouka, *Chem. Commun.*, 2019, **55**, 2007–2014.
19 S. Topman, D. Tamir-Ariel, H. Bochnic-Tamir, T. Stern Bauer, S. Shafir, S. Burdman and Z. Hayouka, *Microb. Biotechnol.*, 2018, **11**, 1027–1036.
20 R. C. Bennett, M. W. Oh, S. H. Kuo, Y. Belo, B. Maron, E. Malach, J. Lin, Z. Hayouka and G. W. Lau, *ACS Infect. Dis.*, 2021, **7**, 672–680.
21 H. E. Caraway, J. Z. Lau, B. Maron, M. W. Oh, Y. Belo, A. Brill, E. Malach, N. Ismail, Z. Hayouka and G. W. Lau, *Antibiotics*, 2022, **11**, 413.
22 B. Maron, J. Rolff, J. Friedman and Z. Hayouka, *Microbiol. Spectr.*, 2022, **10**, e00973–22.
23 B. Antunes, C. Zanchi, P. R. Johnston, B. Maron, C. Witzany, R. Regoes, Z. Hayouka and J. Rolff, *PLoS Biol.*, 2024, **22**, e3002692.
24 H. Cheriker, T. Stern Bauer, Y. Oren, S. Nir and Z. Hayouka, *Chem. Commun.*, 2020, **56**, 11022–11025.
25 T. Stern Bauer, R. Yakobi, M. Hurevich, S. Yitzchaik and Z. Hayouka, *Sensors*, 2023, **23**, 561.
26 A. D. Williams, E. Portelius, I. Kheterpal, J. T. Guo, K. D. Cook, Y. Xu and R. Wetzel, *J. Mol. Biol.*, 2004, **335**, 833–842.
27 G. De Baets and J. Van Durme, *J. Mol. Biol.*, 2014, **426**, 2405–2412.
28 M. Cardamone and N. K. Puri, *Biochem. J.*, 1992, **282**, 589–593.
29 V. N. Uversky, S. Winter and G. Löber, *Biophys. Chem.*, 1996, **60**, 79–88.
30 C. A. Species, B. Bolognesi, J. R. Kumita, T. P. Barros, E. K. Esbjorner, L. M. Luheshi, D. C. Crowther, M. R. Wilson, C. M. Dobson, G. Favrin, J. J. Yerbury, E. K. Esbjörner and M. Leila, *ACS Chem. Biol.*, 2010, **5**, 735–740.
31 B. Mannini, E. Mulvihill, C. Sgromo, R. Cascella, R. Khodarahmi, M. Ramazzotti, C. M. Dobson, C. Cecchi and F. Chiti, *ACS Chem. Biol.*, 2014, **9**, 2309–2317.
32 T. Garfagnini, F. Bemporad, D. Harries, F. Chiti and A. Friedler, *J. Mol. Biol.*, 2023, **435**, 168281.
33 T. Garfagnini, Y. Levi-Kalisman, D. Harries and A. Friedler, *Biophys. J.*, 2021, **120**, 3455–3469.

34 J. P. Gallivan and D. A. Dougherty, *Proc. Natl. Acad. Sci. U. S. A.*, 1999, **96**, 9459–9464.
35 G. Tesei, M. Vazdar, M. Ringkjøbing Jensen, C. Cragnell, P. E. Mason, J. Heyda, M. Skepo, P. Jungwirth and M. Lund, *Proc. Natl. Acad. Sci. U. S. A.*, 2017, **114**, 11428–11433.
36 C. C. Decandio, E. R. Silva, I. W. Hamley, V. Castelletto, M. S. Liberato, V. X. Oliveira, C. L. P. Oliveira and W. A. Alves, *Langmuir*, 2015, **31**, 4513–4523.
37 M. A. Roseman, *J. Mol. Biol.*, 1988, **200**, 513–522.
38 I. N. Shalova, I. N. Naletova, L. Saso, V. I. Muronetz and V. A. Izumrudov, *Macromol. Biosci.*, 2007, **7**, 929–939.
39 J. I. Austerberry, R. Dajani, S. Panova, D. Roberts, A. P. Golovanov, A. Pluen, C. F. van der Walle, S. Uddin, J. Warwicker, J. P. Derrick and R. Curtis, *Eur. J. Pharm. Biopharm.*, 2017, **115**, 18–30.
40 J. I. Austerberry, A. Thistlethwaite, K. Fisher, A. P. Golovanov, A. Pluen, R. Esfandiary, C. F. Van Der Walle, J. Warwicker, J. P. Derrick and R. Curtis, *Biochemistry*, 2019, **58**, 3413–3421.
41 P. I. Semenyuk, L. P. Kurochkina, N. B. Gusev, V. A. Izumrudov and V. I. Muronetz, *Biochem. Biophys. Res. Commun.*, 2017, **489**, 200–205.
42 A. A. Sofronova, V. A. Izumrudov, V. I. Muronetz and P. I. Semenyuk, *Polymer*, 2017, **108**, 281–287.
43 A. Stevens and R. C. Augusteyn, *Eur. J. Biochem.*, 1997, **243**, 792–797.